

Atomistic cluster alignment method for local order mining in liquids and glassesX. W. Fang,^{1,2} C. Z. Wang,^{2,*} Y. X. Yao,² Z. J. Ding,¹ and K. M. Ho²¹*Hefei National Laboratory for Physical Sciences at Microscale and Department of Physics, University of Science and Technology of China, Hefei, Anhui 230026, People's Republic of China*²*Ames Laboratory, US Department of Energy and Department of Physics, Iowa State University, Ames, Iowa 50011, USA*
(Received 14 June 2010; revised manuscript received 23 August 2010; published 16 November 2010)

An atomistic cluster alignment method is developed to identify and characterize the local atomic structural order in liquids and glasses. With the “order mining” idea for structurally disordered systems, the method can detect the presence of any type of local order in the system and can quantify the structural similarity between a given set of templates and the aligned clusters in a systematic and unbiased manner. Moreover, population analysis can also be carried out for various types of clusters in the system. The advantages of the method in comparison with other previously developed analysis methods are illustrated by performing the structural analysis for four prototype systems (i.e., pure Al, pure Zr, $Zr_{35}Cu_{65}$, and $Zr_{36}Ni_{64}$). The results show that the cluster alignment method can identify various types of short-range orders (SROs) in these systems correctly while some of these SROs are difficult to capture by most of the currently available analysis methods (e.g., Voronoi tessellation method). Such a full three-dimensional atomistic analysis method is generic and can be applied to describe the magnitude and nature of noncrystalline ordering in many disordered systems.

DOI: [10.1103/PhysRevB.82.184204](https://doi.org/10.1103/PhysRevB.82.184204)

PACS number(s): 06.30.Bp, 61.20.Ja, 61.20.Gy, 61.25.Mv

I. INTRODUCTION

Knowledge about the local atomic packing order in metallic liquids and glasses is critical for understanding and controlling the transformation pathways in metallic alloys upon rapid cooling from the high-temperature liquids.¹ However, structural description of disordered systems, such as metallic liquids and glasses, has been a long-standing challenge. Even detailed atomic coordinates of liquids and glasses can be available from reliable computer simulations,^{2–4} the underlying structural orders in these systems are not easy to discern because of the lack of long-range order.

Currently, the most commonly used methods in analyzing local orders in liquids and glasses include the bond-orientation order (BOO) method,⁵ Honeycutt-Anderson (HA) common neighbor analysis,^{6–8} and Voronoi tessellation method.^{9,10} Although these methods, coupled with pair correlations, have provided important insights into the structures of a number of noncrystalline materials, reliable and robust descriptors to characterize various types of short-range orders (SROs) in noncrystalline systems are still lacking.

BOO analysis is mathematically elegant but it is too sensitive to the structure distortion and the signals of various local orders in the liquids and glasses are not easy to extract. The HA method which classifies the atom pairs according to common neighbors shared by the pair of atoms, on the other hand, is robust to structure distortions, but it gives only partial information about the whole atomic packing in the SRO structures. For example, the HA index of (1551) is commonly referred to as a signature of icosahedral SRO (ISRO) in the literature.⁴ However, it should be noted that the structure unit with the HA index of (1551) is a pentagonal bipyramid which is only a fragment (seven atoms) of a 13-atom icosahedral cluster. A large fraction of HA-(1551) unit in the sample is a necessary but not a sufficient condition for the presence of ISRO in the system. A prototype example is the

C16 structure of Zr_2Ni which has a large fraction (about 50%) of (1551)-HA units, but the C16 structure is clearly nonicosahedral.¹¹ Therefore, the HA common neighbor analysis, though simple and robust with respect to the atomic distortion, is not a sufficient indicator for the SRO in liquids and glasses.

Voronoi tessellation method divides space into polyhedra around atoms by construction of bisecting planes along the lines joining the central atom and all its neighbors.^{9,10} A Voronoi index $\langle n_3, n_4, n_5, n_6, \dots \rangle$ associated with the polyhedron is used to characterize the topology of the local atomic packing structure, where n_i denotes the number of i -edged faces of the Voronoi polyhedron around the central atom. By dividing the space into various polyhedra centered at each atom, Voronoi tessellation method classifies the local atomic structures according to the Voronoi index. Although this method is mathematically rigorous, there is some ambiguity when applying to physical systems. Because Voronoi tessellation has different tolerance for different geometric structures, it is hard to determine a universal criterion to remove small faces resulting from the thermal fluctuations on different clusters. For example, it is very difficult to identify face-centered-cubic (fcc) and hexagonal close-packed (hcp) type of local structures using the Voronoi tessellation method because the Voronoi index of these structures ($\langle 0, 12, 0, 0 \rangle$) can change dramatically due to even very small structure distortions.¹² Moreover, the Voronoi index does not provide an intuitive view of the local structure in real space and it is not clear how closely related are the structures of the clusters with the same Voronoi index, which may hinder our understanding of the effects of the local structural order on the dynamical as well as other properties of the liquids and glasses.

In this paper, we developed an atomistic cluster alignment method to identify and characterize the local structure order in metallic liquids and glasses using only the atomistic coordinates information. All the structural information is well maintained without any error adjustment procedure, which

makes this “order mining” technique very useful in many structurally disordered systems. Applications of this method to some prototype systems have demonstrated the advantages of the new method over the existing methods for local structure analysis. In Sec II, details of the cluster alignment method will be described. Applications of the alignment method to prototype elementary and binary metallic liquids will be presented and discussed in Sec III. In Sec IV, comparison with the commonly used Voronoi tessellation analysis will be given. Finally, conclusions will be presented in Sec V.

II. CLUSTER ALIGNMENT METHOD

In our alignment scheme, we characterize the local environment of each atom in the sample by an atomic cluster which includes the atom itself and its nearest neighbors. Operationally, we include all atoms within a distance equal to the first minimum in the total radial distribution function. The total number of such clusters is equal to the number of atoms in the sample, and each local cluster contains about 15–19 atoms. These clusters are interpenetrated in real space. The alignment is performed on such clusters instead of directly on the whole molecular dynamics (MD) configuration. For binary alloys, we divide the clusters into subsets according to the chemical constituent of the center atom. Three types of alignments are performed in this study: (1) a *collective alignment* to detect if there are any SROs in the system; (2) a *template alignment* on the collective-alignment result to further identify what are the major SROs; and (3) an *individual cluster-template alignment* to determine the population (fraction) of each type of SROs. In the following sections, these three types of alignment schemes will be described in more detail.

A. Collective alignment

In the collective alignment, the clusters in the same subset (according to the chemical constituent of the center atom) are aligned with each other to minimize the overall mean-square distances between different clusters. The clusters are rigidly rotated and translated relatively to each other during the alignment. To carry out this alignment, a simulated annealing scheme implemented with MD simulation is employed. The results of this alignment will reveal the common structural motif characterizing the local environment of a given chemical constituent. The use of the MD scheme permits the alignments of all the clusters in the subsets to be done simultaneously to obtain a consensus motif in an efficient manner.

In the MD alignment simulations a modified Lenard-Jones-type attractive potential is used to describe the attractive interaction between the atoms in different local clusters,

$$V_{im,jn}(r) = -0.04 \times \epsilon \times \left(\frac{\sigma^2}{r_{im,jn}^2 + \Delta} \right)^3, \quad (1)$$

where $V_{im,jn}$ is the attractive potential between atom m in cluster i and atom n in cluster j ($i \neq j$), and $r_{im,jn}$ is the distance between atom m in cluster i and atom n in cluster j . The reduce unit is used in the simulation: the unit of energy

is set to ϵ as shown in Eq. (1); the unit of length between two atoms is set to σ , ($\sigma=1.0$ Å); the mass of each atom is set to 1 (the influence of chemical specie is not taken into consideration in the present scheme but it can be included in a straightforward way). The cutoff distance for the attractive interaction $V_{im,jn}$ is set to be 1.0σ and the parameter Δ in Eq. (1) is set to $0.5\sigma^2$.

A strong harmonic potential is also introduced between atom pairs within the same cluster to keep the structure quasi-rigid during the collective-alignment process,

$$U_{m,n} = -\frac{1}{2}K \times (r_{m,n} - r_{m,n}^0)^2, \quad (2)$$

where $U_{m,n}$ is the strong harmonic potential between atom m and atom n , and the $r_{m,n}$ is the distance between atom m and atom n in the same cluster. $r_{m,n}^0$ is the initial distance between atom m and n before alignment. A force constant $K=4.0 \times 10^4 \epsilon/\sigma^2$ is large enough to guarantee that the geometric distortions of each cluster during the alignment are negligible.

Using the two interatomic potentials described above, MD simulated annealing is performed. In the beginning of the MD simulation, all clusters' center atoms are shifted to overlap at the center of the simulation cell. Then the temperature of system is raised to $T=0.125\epsilon/K_B$ (Ref. 13) (K_B is Boltzmann constant) to achieve thermal equilibrium. Using the velocity scaling scheme which scales each atom's velocity by a factor of 0.98 every 20 MD steps, the temperature of the system is slowly cooled down to approximately zero temperature in 10 000 time steps. Although, in principle, all the clusters in a subset can be used in the collective alignment, in practice we found that 2000 local clusters randomly selected from each subset provide sufficient statistical sampling of the SRO in liquids and glasses.

As an example, the result of the collective alignment for a $Zr_{35}Cu_{65}$ glass model at 300 K is illustrated in Fig. 1. The alignment is performed using 2000 Cu-centered local clusters randomly selected from molecular-dynamics simulation trajectories. Before the collective alignment, the atoms are distributed uniformly around a sphere corresponding to the first peak in pair correlation function $g(r)$ as shown in Fig. 1(a). After alignment, a distinct icosahedral pattern showed up in Fig. 1(b), indicating that most local clusters have icosahedral structural motifs and icosahedral is the strongest SRO in this system.

In order to see the alignment results more clearly, a Gaussian smearing scheme is used to convert the atomic distribution after the alignment into atomic density in three-dimensional space as shown in Fig. 1(d),

$$D(\vec{r}) = \frac{1}{m} \times \sum_{i=1}^{m \times n} \left(\frac{\alpha}{\pi} \right)^{3/2} e^{-\alpha \times (\vec{r} - \vec{r}_i)^2}, \quad (3)$$

where \vec{r}_i is the position vector of atom i , m is the number of local clusters used in the alignment (2000 in the present case), and n is the number of atoms per cluster (16 in the present case).

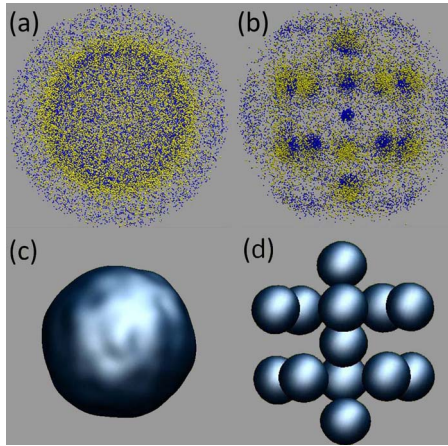


FIG. 1. (Color online) An example of collective alignment with 2000 Cu-centered clusters from undercooled liquid $Zr_{35}Cu_{65}$ at 300 K. Each cluster contains one Cu center atom and 15 nearest neighbors. (a) and (b) show the configurations before and after collective alignment, respectively. (c) and (d) are the atomic-density contour plots corresponding to the distribution in (a) and (b), respectively, using the Gaussian smearing scheme of Eq. (3). The isosurface value is 0.141 \AA^{-3} .

B. Template alignment on collective-aligned clusters

The collective alignment described in Sec. II A gives us direct information about whether there is any SRO in the system. A natural follow-up issue is how to characterize the type of SROs from the collective-alignment patterns. This issue can be addressed by checking the structural similarity between the distribution obtained from collective alignment and the templates corresponding to different types of SROs of interest (e.g., icosahedra, fcc, hcp, bcc, etc.). The template alignment described here can serve as a tool to characterize the detailed nature of the SRO in the system.

The template alignment between collective-aligned clusters and a selected template is carried out in the following way. Clusters from collective alignment are brought onto the template with the average position of clusters' centers overlapping the center of the template. Then alignment between the template and the clusters is performed by rotating and translating the template while keeping all the clusters fixed. The interaction potential between the template and the collective-aligned clusters is described by Eq. (1) while the atoms in the template are linked with strong springs as in Eq. (2). In a typical run, the template is randomly rotated, followed by a relaxation with conjugate gradient method to search for the total energy minimum for the interaction between the template and all clusters in the system as described in Eq. (4),

$$V = \frac{1}{n_s} \times \sum_{i=1}^{n_s} \sum_{m=1}^{n_C} \sum_{k=1}^{n_T} \left[-0.04 \times \epsilon \times \left(\frac{\sigma^2}{r_{im,k}^2 + \Delta} \right) \right], \quad (4)$$

where V is the attractive potential energy per cluster, $r_{im,k}$ is the distance between atom m in cluster i and atom k in the template, $n_T(n_C)$ is the number of atoms in the template (cluster), and n_s ($=2000$ in present study) is the total number

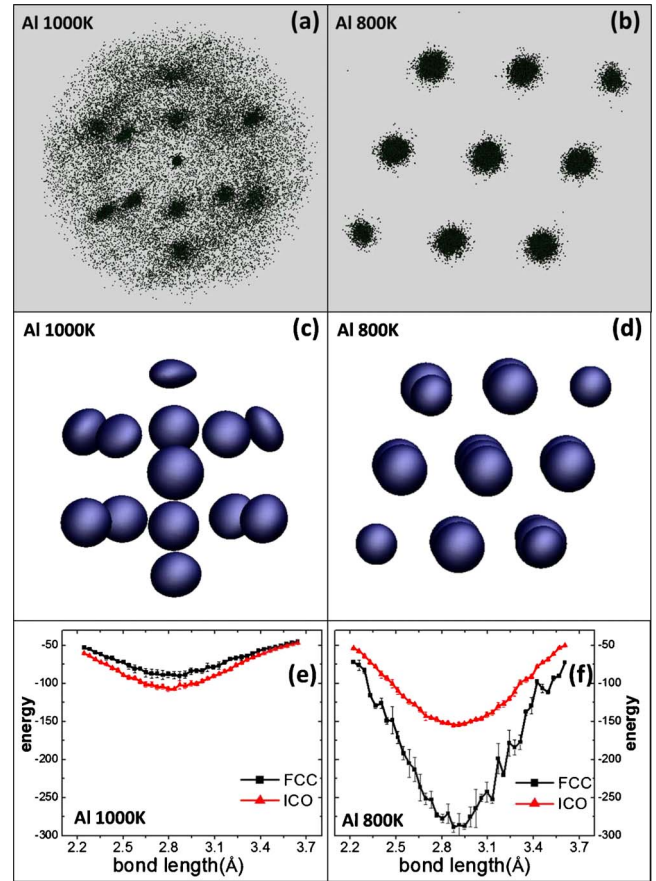


FIG. 2. (Color online) The final configurations of the collective alignments and the results of template alignments for pure Al at 1000 K and 800 K, respectively. (a) and (b) are the atomic configuration at these two temperatures. (c) and (d) are the corresponding atomic-density contour plots with an isosurface value of 0.141 \AA^{-3} . (e) and (f) are the attractive potential energies [defined by Eq. (4)] as the function of bond length for fcc and icosahedral type of short-range orders at the two temperatures.

of local clusters selected in the collective-alignment simulation. The cut-off distance for calculating the total energy V is set to 1.0σ , and the parameter Δ is set to $0.5\sigma^2$. Lower attractive potential energy in this template alignment indicates a better structural fit (similarity) between the template and the aligned set of clusters. For each alignment we tried 1000 runs with different initial rotations and the lowest-energy try from these runs determines the best alignment. Meanwhile, we can obtain the optimized bond length for each template by tuning its bond length to further minimize the attractive energy as shown in Figs. 2(e) and 2(f), respectively. This attractive potential energy versus bond-length curve qualitatively measures the similarity between each template and the aligned set of clusters, thus the strength of the corresponding SRO in the system.

C. Individual cluster-template alignment

Population-based analysis is widely used to study the structural and dynamical properties of metallic liquids and glasses.^{14,15} In our cluster alignment method, the population

of different SROs can be described by classifying the clusters in the system into various types of SRO according to their structural similarity with the given templates. The optimum bond length of the template can be obtained from the template-alignment described above.

In this individual cluster-template alignment process, the templates are used to perform alignment with each local cluster in the sample. In this step, the alignment only includes a template and one local cluster at a time. The same harmonic potential described in Sec. II A is adopted to maintain the structures of the cluster quasirigid during the alignment. However, because the alignment here is one-on-one (not one-on-many as in Sec. II B), a much stronger attractive potential between the cluster and the template is used to give satisfactory alignment results. As shown in Eq. (5), the attractive potentials used in the individual cluster-template alignment have the same form and the same values of the parameters as that in Eq. (1) except that the interaction strength is 100 times larger (i.e., replace the prefactor 0.04 by 4.0),

$$V_{im,jn}(r) = -4.0 \times \epsilon \times \left(\frac{\sigma^2}{r_{im,jn}^2 + \Delta} \right)^3. \quad (5)$$

In a typical run of individual cluster-template alignment, the template is fixed, and the selected single cluster is randomly rotated followed by relaxation under the potentials discussed above. Although the total attractive potential energy after the alignment can be used to measure the structural fitness of the alignment, we find that a direct structure fitting score f , defined as the minimal square distance between the template and the cluster after the relaxation, is more straightforward to describe the structural similarity between the template and the aligned cluster,

$$\Delta r_T^2 = \min'_{C=1, \dots, n_C} \Delta r_{C,T}^2, \quad (6)$$

$$f = \min_{\{r_c\}} \left(\frac{1}{n_{TT=1}} \sum_{n_T} \Delta r_T^2 \right),$$

where $\Delta r_{C,T}^2$ is the distance between atom C in the cluster and atom T in the template. Δr_T^2 is the minimal square distance between atom T in the template and all n_C atoms in the cluster with a constraint that each atom in the cluster is counted no more than once ($n_C > n_T$).

In order to get the global optimum alignment configuration between the cluster and the template, we tried 4000 alignment runs with different random initial rotations for each cluster selected from the sample and the final fitting score F , defined as the minimum score from these 4000 alignments as shown in Eq. (7), is used to measure the structural similarity between the cluster and the template,

$$F = \min(f_i) \quad (i = 1, \dots, 4000). \quad (7)$$

If the fitting score F is smaller than a cut-off score F_C ,

$$F_C = \frac{1}{n_{TT=1}} \sum_{n_T} (r_0^T \times 20\%)^2, \quad (8)$$

where r_0^T is the bond length between center atom and its neighbor atom T in the corresponding optimized template, the cluster is considered to be structurally similar to the template. In our classification scheme, the cut-off fitting score F_C is fairly close to the full width at half maximum of the first peak in the pair-correlation function for each system.

III. APPLICATION EXAMPLES

We demonstrate our cluster alignment method by applying it to elemental Al, Zr liquids as well as binary $Zr_{35}Cu_{65}$ and $Zr_{36}Ni_{64}$ alloys. These samples are chosen to represent a wide variety of atomic structures corresponding to different types of SRO. These results demonstrate the versatility of our method in local order analysis.

All the samples were prepared by *ab initio* molecular-dynamics simulations within density-functional theory as implemented in the Vienna *ab initio* simulation package.¹⁶⁻¹⁸ Single Γ point was used for the K point sampling and all the calculations were carried out in the *NVT* ensemble with Nose thermostat. A time step of 3 *fs* was used with verlet algorithm for time integration of Newton's equations of motion.

A. Liquid-crystal transition in Al

The simulation of Al system was performed using a 108-atom cubic unit cell with periodic boundary conditions. Test simulation of 256 atoms Al samples show the similar result. The liquid was first prepared at 1500 K (well above the melting point of 937 K), then cooled down to 1000 K and 800 K with a cooling rate of 100 K per 1000 time steps. After the system reached thermal equilibrium, an additional 16 000 time steps were performed to collect the trajectory for analysis. To set up the cluster sample pool, one in every 64 frames was selected from the MD simulation trajectories to avoid memory effects.

Figure 2(a) shows the result of the collective alignment of 2000 local clusters randomly selected from Al liquid at 1000 K. Each cluster contains one center atom and 15 nearest neighbors. Each point in the figure denotes an atom. The figure shows 13 high-density disjoint regions arranged in a clear icosahedral-like pattern. This alignment pattern provides direct evidence of strong icosahedral order in Al liquid, consistent with the energetics of Al local clusters in metallic liquid environment from first-principles embedded-cluster calculations.¹⁹ At 800 K, since the system has already crystallized, the collective-alignment result exhibits fcc order as shown in Fig. 2(b). It should be noted that fcc order is very difficult to pick up by the widely used Voronoi tessellation method but our collective-alignment method works well even in the fcc crystal limit. Figures 2(c) and 2(d) show the atomic-density contour plots with an isosurface value of 0.141 \AA^{-3} (σ^{-3}) for the Al sample at 1000 K and 800 K, respectively. It is very clear from the figures that at high temperature the system exhibits icosahedral order while at low temperature the system is dominated by the fcc order.

TABLE I. The populations of local clusters with different SROs by individual cluster-template alignment. The template was optimized by the template-alignment procedure and the individual cluster-template alignment was carried out for each local cluster in the samples. The populations of different SROs were obtained by using the fitting score criterion F_c as defined in Sec. II C. The population of local clusters with index $\langle 0, 0, 12, 0 \rangle$ by Voronoi tessellation was also presented for the purpose of comparison.

System	fcc (%)	hcp (%)	bcc (%)	Icosahedra (%)	Z15 (%)	$\langle 0, 0, 12, 0 \rangle$ (%)
Al 1000 K	1.11	1.96	0.27	2.34		0.51
Al 800 K	97.99	11.4	7.63	4.70		0.33
Zr 2400 K	1.01	3.01	2.17	2.97		0.23
Zr 2135 K	1.64	3.45	4.97	4.73		0.89
Cu center $Zr_{35}Cu_{65}$ 1100 K	0.62	3.41	0.21	9.98		2.37
Zr center $Zr_{35}Cu_{65}$ 1100 K	2.18	4.96	3.00	2.99	4.35	0.03
Ni center $Zr_{36}Ni_{64}$ 1100 K	0.65	1.93	1.65	3.86		1.29
Zr center $Zr_{36}Ni_{64}$ 1100 K	0.58	2.51	2.13	1.89	1.71	0.0

From the collective-alignment results of pure Al, we can see that the short-range order is mainly icosahedral at 1000 K and fcc at 800 K. Based on the collective-alignment results, the template alignment is then performed to yield the potential energy versus bond-length curves for icosahedral type and fcc type of SRO, respectively. The results are shown in Figs. 2(e) and 2(f), respectively, for the two temperatures, which quantitatively characterize the strength of the two different types of SRO in the system. In Fig. 2(e) the curve for icosahedral SRO is slightly lower than that for the fcc SRO, indicating a relatively stronger icosahedral SRO in Al liquid at 1000 K. On the other hand, Fig. 2(f) shows that the curve of fcc SRO is much lower than that of icosahedral SRO, indicating a much stronger fcc order, consistent with the fact that the sample has crystallized into an fcc crystal.

The competing between the icosahedral and fcc SRO upon cooling from the liquid can be further illustrated by the individual cluster-template alignment as shown in Table I. Although the icosahedral SRO is stronger at 1000 K, a small fraction of fcc local clusters (about 1.11%) is also presented. As the temperature is reduced to 800 K, the population of the fcc SRO increases dramatically from 1.11% to 97.99%. It should be noted that the geometric structure of fcc cluster and that of icosahedral cluster are similar to some extent.²⁰ As a result, we can still find a small fraction (about 4.7%) of icosahedral-like local clusters at 800 K, which shows the population overlap between icosahedral and fcc SRO due to thermal vibrations.

B. Liquid Zr

Next, we tested our scheme on pure Zr liquid in which competition among several types of structures makes the description of SRO in the system more complicated than the case of pure Al. It has been reported that Zr liquid exhibits various types of SROs including bcc, hcp, and icosahedral SROs.^{4,21,22} A liquid sample of 100 atoms was prepared at 2500 K and then cooled down to 2400 K and 2135 K with the same cooling rate as for pure Al studied in Sec. III A. 2000 additional MD steps were carried out after the system

was thermally equilibrated and one in every ten frames was selected to construct the cluster database for the analysis.

Figure 3(a) shows the collective-alignment result of Zr liquid at 2400 K, which exhibits only a few high-density spots without a clearly ordered pattern. For undercooled Zr liquid at 2135 K, more high-density regions appeared as shown in Fig. 3(b) and a bcc order start to emerge from the aligned pattern. This can be more clearly seen in the corresponding atomic-density contours as shown in Fig. 3(d).

The template-alignment results for the liquid Zr at 2400 K and 2135 K are shown in Figs. 3(e) and 3(f), respectively. We note that a bcc template up to second neighbor shell would include 15 atoms (one center atom plus eight first shell neighbors plus six shell neighbors), which is two atoms more than icosahedral and fcc template. Since the attractive potential energy sums over the contributions from all the atoms in the template, consequently the total number of atoms for each template should be same if we want to compare the fitness between the various templates and collective-aligned clusters. Thus we choose to modify the bcc template by removing two atoms in the second shell. Our tests show that this modification does not affect the optimized bond length of the bcc template. The attractive potential energy of this modified bcc template is found to be comparable with the other two templates from template alignment.²³ Figures 3(e) and 3(f) show that none of the icosahedral, fcc, or bcc SRO is dominate at either 2400 or 2135 K, although at the lower temperature, 2135 K, the collective-aligned configuration is a little in favor of bcc and icosahedra SROs. The population of these three types of short-range orders from our individual cluster-template alignment is shown in Table I. We can see the promotions of all the three types of SROs (icosahedra, bcc, and hcp) are increased as temperature decreases. It is interesting to see that bcc SRO increases much faster than the others. Compared to previous analysis of SRO in Zr liquid,⁴ our present approach provides a more physical scheme for classification of various types of SROs in a straightforward way in this complex system.

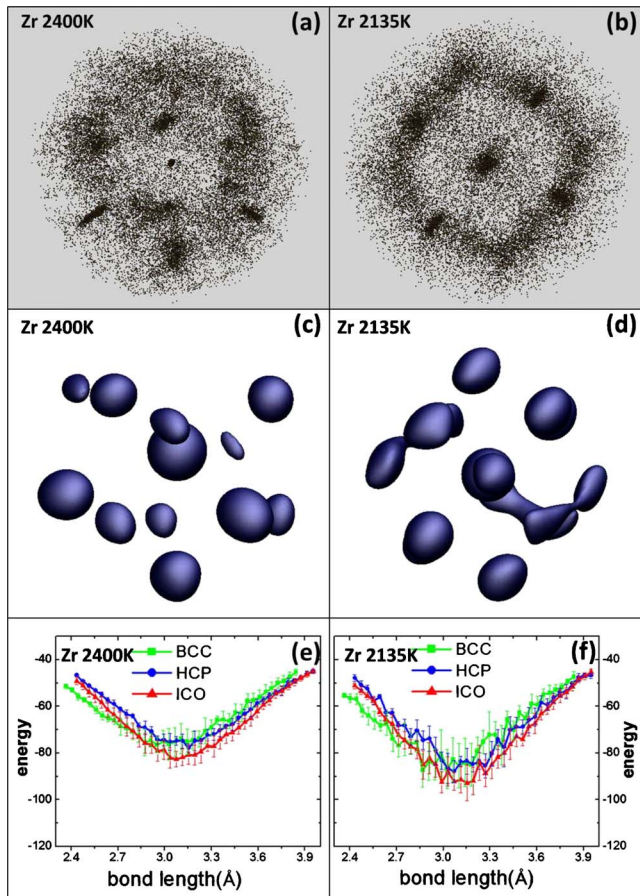


FIG. 3. (Color online) The final configurations of collective alignments and the results of template alignments for pure Zr at 2400 and 2135 K. (a) and (b) are the atomic configurations, (c) and (d) are the corresponding atomic-density contour plots with an isosurface value of 0.141 \AA^{-3} . (e) and (f) are the attractive potential energies as the function of bond length for bcc, hcp, and icosahedral type of short-range orders.

C. Cluster alignment for $\text{Zr}_{35}\text{Cu}_{65}$ and $\text{Zr}_{36}\text{Ni}_{64}$ undercooled liquids

Our cluster alignment method can also be applied to multicomponents systems. We choose $\text{Zr}_{35}\text{Cu}_{65}$ and $\text{Zr}_{36}\text{Ni}_{64}$ undercooled liquids as two examples. Zr-Cu binary system has good glass formability and has attracted a lot of attention from experiment and simulation studies.^{11,14,15,24–32} Icosahedral SRO has been recognized to be critical for the liquid-glass transition in this system. Meanwhile, studies show that the glass formability of Zr-Ni binary is not as good as Zr-Cu although Ni and Cu are neighbors in the periodic table and the atomic size ratios between Zr:Ni and Zr:Cu are very similar.^{28,29,31}

Ab initio MD simulations were performed with unit cells contain 100 atoms and with periodic boundary conditions. Test simulation with 200 atoms for the $\text{Zr}_{35}\text{Cu}_{65}$ system gives results similar to those with 100 atoms. Both $\text{Zr}_{35}\text{Cu}_{65}$ and $\text{Zr}_{36}\text{Ni}_{64}$ systems were initially prepared at 2500 K, followed by cooling to 1100 K with a cooling rate of 100 K per 1000 MD steps. An additional 12 000 time steps were performed and the coordinates of the atoms in every 30 MD steps were used for analysis.

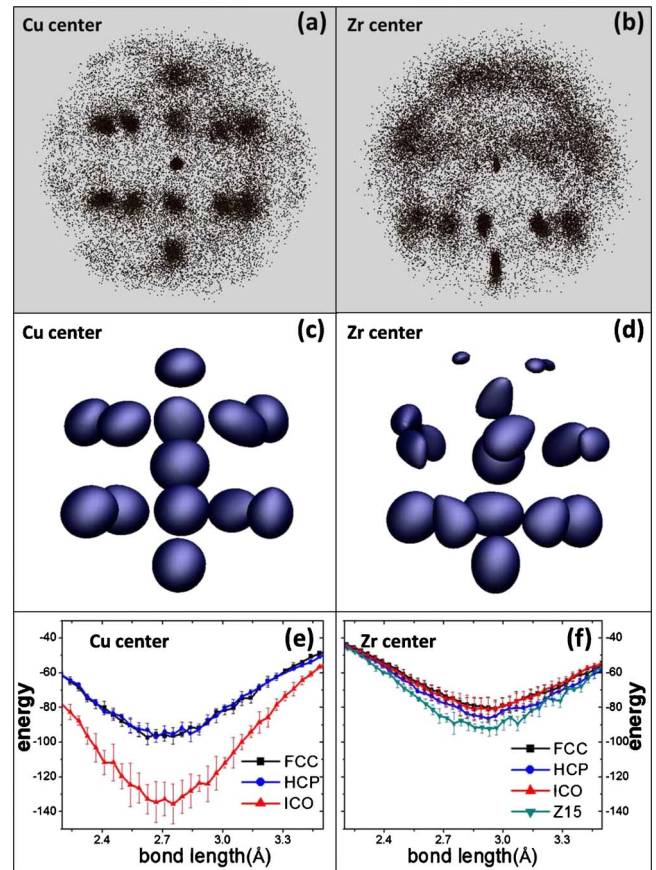


FIG. 4. (Color online) The final configurations of collective alignments and the results of template alignments for $\text{Zr}_{35}\text{Cu}_{65}$ undercooled liquid at 1100 K. (a) and (b) are the atomic configurations for Cu-center and Zr-center local clusters, (c) and (d) are the corresponding atomic-density contour plots with an isosurface value of 0.141 \AA^{-3} . (e) and (f) are the attractive potential energies as the function of bond-length curves for fcc, hcp, Z15, and icosahedral type of short-range orders.

The collective alignments are performed separately for local clusters with different chemical specie in the center, since different types of center atoms may have different local orders. Figures 4(a) and 4(c) show a clear icosahedral pattern for the Cu-centered clusters in the $\text{Zr}_{35}\text{Cu}_{65}$ liquid at 1100 K, consistent with previous studies.¹¹ At the same temperature, we can identify only a very weak icosahedral-like configuration as shown in Figs. 5(a) and 5(c) for Ni-centered local clusters in the $\text{Zr}_{36}\text{Ni}_{64}$ liquid. These results are consistent with Voronoi tessellation and Honeycutt-Anderson analysis results in the literature.^{11,15}

The Zr-centered local clusters in both two systems exhibit only a few high-density regions as shown in Figs. 4(b) and 4(d), respectively. These figures show that there is no dominant structural order in the nearest-neighbor shell of Zr-centered clusters. However, a pentagonal bipyramid [HA index of (1551)] can be found from the collective alignment, as shown in Figs. 4(d) and 5(d), although a complete icosahedral pattern is not observed. In the literature, small clusters with HA index of (1551) have been commonly used as an indicator of ISRO in metallic liquids and glasses. Our result indicates that systems exhibiting strong pentagonal bipyra-

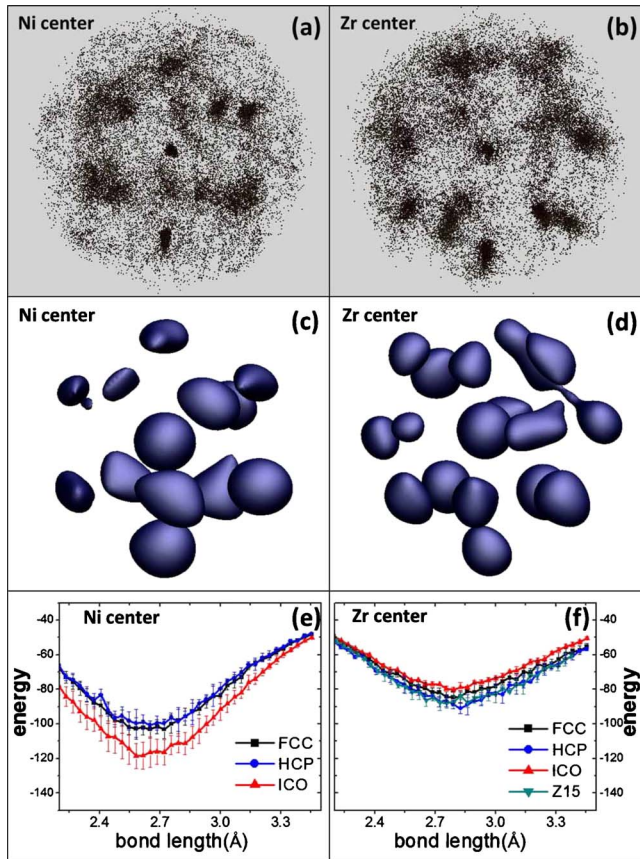


FIG. 5. (Color online) The final configurations of collective alignments and the results of template alignments for $Zr_{36}Ni_{64}$ undercooled liquid at 1100 K. (a) and (b) are the atomistic configurations for Ni-center and Zr-center local clusters, (c) and (d) are the corresponding atomic-density contour plots with an isosurface value of 0.141 \AA^{-3} . (e) and (f) are the attractive potential energies as the function of bond-length curves for fcc, hcp, Z15, and icosahedral type of short-range orders.

mid (1551) order may not have icosahedral SRO.

Template alignments are also carried out for the $Zr_{35}Cu_{65}$ and $Zr_{36}Ni_{64}$ undercooled liquids. In addition to the icosahedral template, we also include templates for hcp and fcc SROs, which might also be important since these are equilibrium crystal structures of the elements involved in these alloys. A Z15-type Frank-Kasper polyhedron^{33,34} is also used as a template for Zr center local environment in the alignment because Zr tends to favor coordination number of 15 in Zr-Cu systems.³⁵ It should be noted that our cluster alignment is not limited to these SROs. Any type of SRO can be taken as template into the analysis if interested. Figure 4(e) shows that the energy curve for icosahedral SRO is much lower than the other two, implying a stronger icosahedral SRO among the three kinds of templates for Cu-centered clusters in $Zr_{35}Cu_{65}$ liquid at 1100 K. Figure 5(e) shows the template-alignment results for Ni center clusters, and we find that although icosahedral SRO is stronger than the other two types, it is much weaker than the icosahedral order in Cu-centered clusters in the $Zr_{35}Cu_{65}$ liquid [Fig. 4(e)]. For Zr-center clusters in both two liquids, the fitting scores of all the four types of SRO templates are relatively low, as shown by

the quite high energy curves in Figs. 4(f) and 5(f). This result is as expected because no obvious order can be seen from the collective-alignment results for Zr-centered clusters in $Zr_{35}Cu_{65}$ and $Zr_{36}Ni_{64}$ liquids shown in Figs. 4 and 5.

As a good binary glass former, the result of individual cluster-template alignment also shows that in the $Zr_{35}Cu_{65}$ undercooled liquid at 1100 K, icosahedral SRO is dominant in Cu-centered clusters (9.98% in population) while about 4.35% Z15-type Frank-Kasper Zr-centered clusters is also observed. In $Zr_{36}Ni_{64}$ at 1100 K, the individual cluster-template alignment also shows a large amount of icosahedral SRO for Ni-centered clusters (3.86%) but not as many as that in $Zr_{35}Cu_{65}$. It is also interesting that we find considerable hcp type local clusters in both $Zr_{35}Cu_{65}$ and $Zr_{36}Ni_{64}$ undercooled liquid at 1100 K (especially in Zr center clusters), which imply that this SRO may also have an important influence in the two liquids.

From the above case studies, we have demonstrated the usefulness of our atomistic cluster alignment method in the study of SRO in noncrystalline systems. From the three alignment steps illustrated above, we can first obtain a pictorial structure description of SRO (collective alignment) for the system, and then carry out quantitative template alignment and individual cluster-template alignment analyses to further quantify the degrees of various SROs of interest in the system.

IV. DISCUSSIONS

A. Classification of local clusters

In our cluster alignment method, the atomic clusters are classified according to their structural similarities to certain templates. To further verify the accuracy of method for clarifying the SRO of the clusters, we show in Fig. 6 the superposition of the atomic structures of all fcc local clusters in pure Al crystalline (800 K), all bcc local clusters in pure Zr liquid (2135 K), and all Cu-centered icosahedral local clusters and Zr-centered hcp local clusters in $Zr_{35}Cu_{65}$ undercooled liquid (1100 K), respectively, obtained from our individual cluster-template alignment scheme. As one can see from the plots, the local clusters belonging to the same SRO from our scheme indeed have similar structures.

We further verify that the local clusters with the same SRO as the template can be picked up by our individual cluster-template alignment. We did this by removing all the selected clusters that belongs to certain SRO from the sample set and reexamining the local order in the rest of the cluster pool. Taking the icosahedra-dominated Cu-centered $Zr_{35}Cu_{65}$ undercooled liquid (1100 K) as an example, after the individual cluster-template alignment, we removed all the icosahedral-type clusters from the sample pool. And then the collective alignment is performed again for the rest clusters in the pool. Figure 7 compares the two collective-alignment results before and after the removal of icosahedral-type clusters. We find that the collective-alignment result of the later one [Fig. 7(b)] is no longer an icosahedral configuration, which demonstrates the sufficiency of our cluster classification scheme. The strong tetrahedral pattern in Fig. 7(b) implies the existence of some degree of hcp SRO in the local

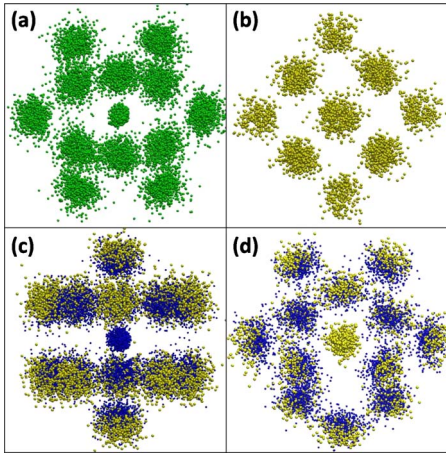


FIG. 6. (Color online) Local clusters that belong to the same type of short-range orders by our individual cluster-template alignment scheme were plot together to see the structural similarity among them. (a) shows the fcc-type clusters in Al at 800 K; (b) shows the bcc type of clusters in Zr undercooled liquid (2135 K); (c) and (d) show the Cu-centered icosahedral-type clusters and the Zr-centered hcp-type clusters in $Zr_{35}Cu_{65}$ undercooled liquid at 1100 K, respectively [yellow(light) points stand for Zr atoms and blue(dark) points stand for Cu atoms].

environment of Cu center species, which is consistent with our individual cluster-template alignment results as shown in Table I.

B. Comparison with Voronoi tessellation analysis

It is also interesting to compare the results from our individual cluster-template alignment scheme with those from the popular Voronoi tessellation method. In Voronoi tessellation analysis, local clusters are classified by Voronoi indices, and then the population is analyzed using these indices rather than real atomic structures. There are two main problems with the Voronoi tessellation. First, structural information such as bond length and bond angles in the clusters is lost when mapping a cluster to a Voronoi index. One-to-one correspondence between a given type of atomic cluster and Voronoi index is not always guaranteed. Furthermore, Voronoi tessellation has different tolerance on structural distortions for different type of clusters. Because of these limi-

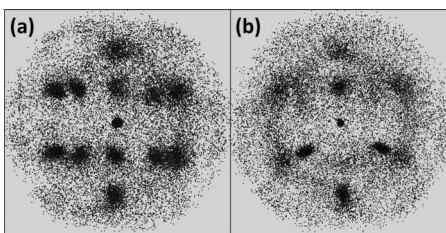


FIG. 7. Collective-alignment results for the cluster pools (a) before and (b) after the icosahedral clusters (identified by the individual cluster-template alignment scheme) have been removed. The data set is Cu-centered clusters in $Zr_{35}Cu_{65}$ undercooled liquid at 1100 K.

tations, Voronoi tessellation is not a good method for investigating some important structure local orders such as fcc, hcp, and bcc. In contrast to Voronoi tessellation, the classification of local clusters in our method according to a structural fitting score provides a more robust measurement of the geometric similarity between local clusters and various templates, and various types of SROs can be studied simultaneously without any bias.

The difference between our method and Voronoi tessellation method can be seen more clearly in the following cases. For pure Al, the ideal Voronoi index of fcc structure should be $\langle 0, 12, 0, 0 \rangle$, but it is hard to get this index even in crystallized Al at 800 K. Although a modified Voronoi method including small-face/short-edge removal can help to get some $\langle 0, 12, 0, 0 \rangle$, Voronoi tessellation is so sensitive to even a tiny structural deformation in fcc clusters, making the classification hard when the thermal vibration exists. When considering the Zr liquid, the Voronoi tessellation method meets more difficulties because the ideal index of hcp type cluster is also $\langle 0, 12, 0, 0 \rangle$,³⁶ the same as that for fcc-type clusters. The degeneracy of the indices for fcc and hcp order makes the comparison among hcp, fcc, and icosahedral SROs impossible. In contrast, our cluster alignment method is straightforward and effective for all kinds of local clusters, basically because no subtle mathematics/geometry criteria are needed for the classification of SROs. Indeed, our method shows remarkable advantage over Voronoi tessellation in the recognition of these important high symmetry SROs. These highly symmetric SROs usually hold the local minimum in energy landscape and play the key role in the determination of thermodynamic phase of metallic system.

For the Cu/Ni-centered clusters in the $Zr_{35}Cu_{65}$ and $Zr_{36}Ni_{64}$ undercooled liquids, although the Voronoi tessellation analysis also shows that the icosahedral SRO is the dominant type of SRO in the system, consistent with the conclusion from our individual cluster-template alignment analysis, the population of the icosahedral clusters is much less than ours. Moreover, for the much more complicated Zr-centered local environment with coordination number larger than 12, Voronoi analysis can only produce some vague indices such as $\langle 0, 2, 8, 4 \rangle$, $\langle 0, 1, 10, 4 \rangle$, $\langle 0, 2, 8, 6 \rangle$, etc., which do not correspond to clear and unique atomic structures. On the contrary, our cluster alignment method can identify the hcp, fcc, Z15 local clusters as well as the icosahedral type of local clusters, which is very useful for a comprehensive understanding of local structure in metallic liquids and glasses.

To further clarify the differences between the two methods, we have applied these two structural analysis methods to 40 000 local clusters in $Zr_{35}Cu_{65}$ undercooled liquid at 1100 K. The populations of the six most-populated indices from Voronoi tessellation analysis on this data set are shown in Fig. 8. The distribution of the icosahedral clusters among these six indices, respectively, obtained by our individual cluster-template alignment scheme is also shown in the same plot for comparison. We find that most (although not all) clusters with index $\langle 0, 0, 12, 0 \rangle$ are identified as icosahedral in our individual cluster-template alignment. For clusters with “icosahedral-like indices” such as $\langle 1, 0, 9, 3 \rangle$, $\langle 0, 1, 10, 2 \rangle$, and $\langle 0, 2, 8, 2 \rangle$, we also find a noticeable frac-

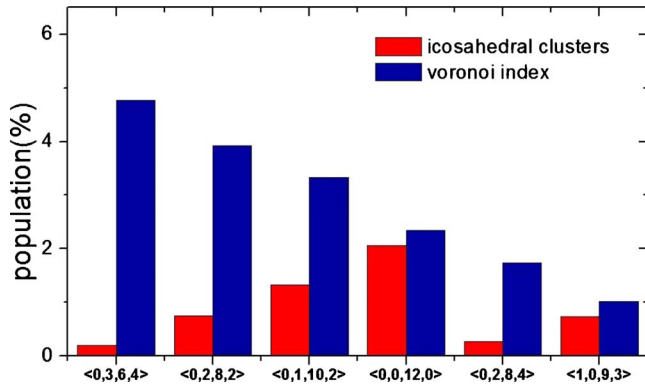


FIG. 8. (Color online) The comparison between results of Voronoi tessellation and individual cluster-template alignment scheme. The data set is 40 000 local clusters (14 000 Zr-centered clusters and 26 000 Cu-centered clusters) in $Zr_{35}Cu_{65}$ undercooled liquid at 1100 K. The plot shows the population of six most Voronoi indices as well as the population of icosahedral type local clusters (classified by individual cluster-template alignment) in these six indices.

tion of them belonging to icosahedral SRO. As shown in Fig. 9, an extra atom (small red) comes in sight of the center atom of an icosahedron from a vertex [Fig. 9(a)] or an edge [Fig. 9(b)] of the icosahedron will create a very small triangular or quadrilateral face at the vertex or edge and transfer

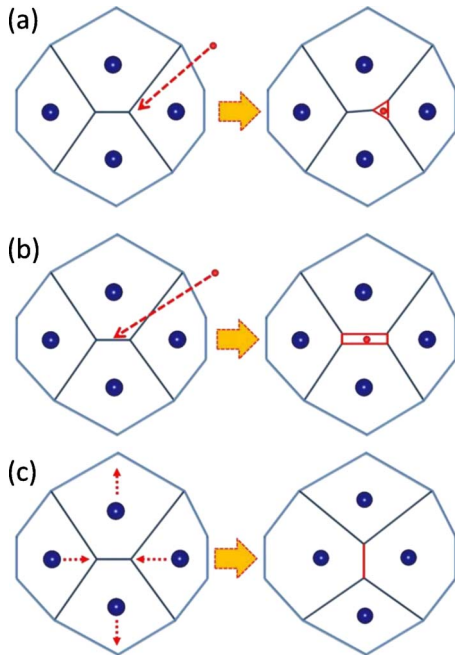


FIG. 9. (Color online) Descriptions of structural transformation between icosahedral and icosahedral-like Voronoi indices. (a) An extra atom (small red atom) comes at a vertex of icosahedron, leading to a $\langle 0,0,12,0 \rangle$ to $\langle 1,0,9,3 \rangle$ transformation (4 pentagons \rightarrow 1 triangle + 1 pentagon + 3 hexagons). (b) An extra atom (small red atom) comes at an edge of icosahedron, leading to a $\langle 0,0,12,0 \rangle$ to $\langle 0,1,10,2 \rangle$ transformation (4 pentagons \rightarrow 1 tetragon + 2 pentagons + 2 hexagons). (c) A small lattice distortion changes the $\langle 0,0,12,0 \rangle$ to $\langle 0,2,8,2 \rangle$ (4 pentagons \rightarrow 2 tetragons + 2 hexagons).

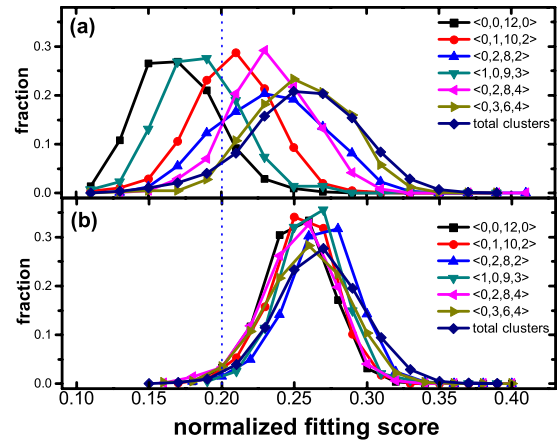


FIG. 10. (Color online) Distribution of the normalized fitting score between (a) the icosahedral and (b) fcc-type templates and local clusters belong to the top six Voronoi indices as well as total clusters in $Zr_{35}Cu_{65}$ undercooled liquid at 1100 K. The data set is the same as that used in Fig. 8. The fitting score for each cluster is normalized by the bond length of template and the dashed line shows the cut-off score for icosahedral SRO in our individual cluster-template alignment scheme.

the index of $\langle 0,0,12,0 \rangle$ into $\langle 1,0,9,3 \rangle$ or $\langle 0,1,10,2 \rangle$ according to Voronoi tessellation method [see Figs. 9(a) and 9(b)]. A small lattice distortion as shown in Fig. 9(c) may also change the $\langle 0,0,12,0 \rangle$ index into $\langle 0,2,8,2 \rangle$. In these situations, when doing population analysis, the results might be more transparent if such fraction of the $\langle 1,0,9,3 \rangle$, $\langle 0,1,10,2 \rangle$, and $\langle 0,2,8,2 \rangle$ indices is classified together with the icosahedral clusters under $\langle 0,0,12,0 \rangle$ rather than separated into different categories in the Voronoi classification.

Figure 10(a) shows the distribution of the normalized fitting score with respect to the icosahedral template from our individual cluster-template alignment scheme for the clusters in the six most-populated Voronoi indices shown in Fig. 8. The dashed line indicates our fitting score criterion (normalized by the bond length of template) used for classification of the clusters. One can see from this plot that under our scheme most but not all of the clusters with index of $\langle 0,0,12,0 \rangle$ can be classified as icosahedral clusters while other indices such as $\langle 1,0,9,3 \rangle$, $\langle 0,1,10,2 \rangle$, and $\langle 0,2,8,2 \rangle$ also contain icosahedral local clusters. From Fig. 10(a), we can clearly see that icosahedral clusters do not exactly corresponding to one Voronoi index, that is, local clusters with same Voronoi index might belong to different structure types. For the purpose of comparison, the distribution of the fitting score for the same six sets of clusters with respect to fcc template is also presented in Fig. 10(b), which shows very little fcc type of SRO in these clusters sets.

V. CONCLUSION

In conclusion, we have developed an atomistic cluster alignment method to study the short-range order in metallic liquids and glasses. This method provides a systematic and straightforward way to determine whether there are any SROs, what type(s) of SROs, and how strong the SROs are

in the system. The population of different types of local clusters can also be obtained using the structural fitting score from individual cluster-template alignment, with which the usual population-based analysis on local structures and dynamics can be carried out.

The key advantage of our new method is that it directly deals with real atomic coordinates of local clusters, which guarantees that structural information is accurately preserved during the analysis to obtain a complete description of short-range order. Successful applications to a variety of systems show that our cluster alignment method is a very important and versatile local structure analysis tool for metallic liquids and glasses.

One interesting thing point to be noted is that with this “real coordinate-based” property, our cluster alignment is a generic order mining method for disordered systems. Local orders can be extracted regardless of the range and degree of the ordering. The alignment can be naturally extended be-

yond the first coordination shell to investigate structural ordering of more coordination shells (i.e., medium-range order) and the percolation of clusters.^{37,38}

ACKNOWLEDGMENTS

We thank S. G. Hao, Li Huang, and S. Y. Wang for useful discussions and providing us their MD simulation trajectories on $Zr_{35}Cu_{65}$, $Zr_{36}Ni_{64}$, and Zr. Work at Ames Laboratory was supported by the U.S. Department of Energy, Basic Energy Sciences, Division of Materials Science and Engineering, including a grant of computer time at the National Energy Research Supercomputing Centre (NERSC) in Berkeley, under Contract No. DE-AC02-07CH11358. X.W.F. acknowledges the support from China Scholarship Council (File No. 2008634035) and Z.J.D. acknowledges the National Natural Science Foundation of China (Grant Nos. 10874160 and 11074232) and “111” project.

*wangcz@ameslab.gov

- ¹H. W. Sheng, W. K. Luo, F. M. Alamgir, J. M. Bai, and E. Ma, *Nature (London)* **439**, 419 (2006).
- ²D. B. Miracle, *Nature Mater.* **3**, 697 (2004).
- ³W. K. Luo, H. W. Sheng, F. M. Alamgir, J. M. Bai, J. H. He, and E. Ma, *Phys. Rev. Lett.* **92**, 145502 (2004).
- ⁴N. Jakse and A. Pasturel, *Phys. Rev. Lett.* **91**, 195501 (2003).
- ⁵P. J. Steinhardt, D. R. Nelson, and M. Ronchetti, *Phys. Rev. B* **28**, 784 (1983).
- ⁶J. D. Honeycutt and H. C. Andersen, *J. Phys. Chem.* **91**, 4950 (1987).
- ⁷P. Ganesh and M. Widom, *Phys. Rev. B* **74**, 134205 (2006).
- ⁸P. Ganesh and M. Widom, *Phys. Rev. B* **77**, 014205 (2008).
- ⁹J. L. Finney, *Nature (London)* **266**, 309 (1977).
- ¹⁰J. L. Finney, *Proc. R. Soc. London, Ser. A* **319**, 479 (1970).
- ¹¹S. G. Hao, M. J. Kramer, C. Z. Wang, K. M. Ho, S. Nandi, A. Kreyssig, A. I. Goldman, V. Wessels, K. K. Sahu, K. F. Kelton, R. W. Hyers, S. M. Caneparri, and J. R. Rogers, *Phys. Rev. B* **79**, 104206 (2009).
- ¹²C. S. Hsu and A. Rahman, *J. Chem. Phys.* **71**, 4974 (1979), see the discussion in the appendix of this paper.
- ¹³Here the reduced unit is performed as this: if time interval $\sigma = 10$ fs and consider system as elementary Al, the start temperature of this annealing scheme is 40 300 K, and the temperature in the end of annealing is 1.6 K.
- ¹⁴Y. Q. Cheng, H. W. Sheng, and E. Ma, *Phys. Rev. B* **78**, 014207 (2008).
- ¹⁵N. Jakse and A. Pasturel, *Phys. Rev. B* **78**, 214204 (2008).
- ¹⁶G. Kresse and J. Hafner, *Phys. Rev. B* **47**, 558 (1993).
- ¹⁷G. Kresse and J. Furthmüller, *Phys. Rev. B* **54**, 11169 (1996).
- ¹⁸The Vienna *ab initio* simulation package (VASP), G. Kresse and J. Furthmüller, *Comput. Mater. Sci.* **6**, 15 (1996).
- ¹⁹Y. X. Yao, C. Z. Wang, and K. M. Ho, *Phys. Rev. B* **76**, 174209 (2007).
- ²⁰A. L. Mackay, *Acta Crystallogr.* **15**, 916 (1962).
- ²¹B. L. Zhang, C. Z. Wang, K. M. Ho, D. Turner, and Y. Y. Ye, *Phys. Rev. Lett.* **74**, 1375 (1995).
- ²²A. Heiming, W. Petry, J. Trampenau, W. Miekeley, and J. Cockcroft, *J. Phys.: Condens. Matter* **4**, 727 (1992).
- ²³We also find that although attractive potential energy for 15-atom bcc template was not comparable with others, the optimized bond length was almost same as that for 13-atom bcc template, which makes our optimized bcc template reliable for the individual cluster-template alignment.
- ²⁴K. Saksli, H. Franz, P. Jvri, K. Klementiev, E. Welter, A. Ehnes, J. Saida, A. Inoue, and J. Z. Jiang, *Appl. Phys. Lett.* **83**, 3924 (2003).
- ²⁵N. Jakse and A. Pasturel, *Appl. Phys. Lett.* **93**, 113104 (2008).
- ²⁶D. H. Xu, B. Lohwongwatana, G. Duan, W. L. Johnson, and C. Garland, *Acta Mater.* **52**, 2621 (2004).
- ²⁷D. Wang, Y. Li, B. B. Sun, K. Lu, and E. Ma, *Appl. Phys. Lett.* **84**, 4029 (2004).
- ²⁸P. Yu, H. Y. Bai, M. B. Tang, and W. L. Wang, *J. Non-Cryst. Solids* **351**, 1328 (2005).
- ²⁹F. Paul and R. Frahm, *Phys. Rev. B* **42**, 10945 (1990).
- ³⁰S. G. Hao, C. Z. Wang, M. J. Kramer, and K. M. Ho, *J. Appl. Phys.* **107**, 053511 (2010).
- ³¹Li Huang, C. Z. Wang, S. G. Hao, M. J. Kramer, and K. M. Ho, *Phys. Rev. B* **81**, 014108 (2010).
- ³²Li Huang, C. Z. Wang, S. G. Hao, M. J. Kramer, and K. M. Ho, *Phys. Rev. B* **81**, 094118 (2010).
- ³³F. C. Frank and J. Kasper, *Acta Crystallogr.* **11**, 184 (1958).
- ³⁴D. R. Nelson, *Phys. Rev. B* **28**, 5515 (1983).
- ³⁵J. Basu and S. Ranganathan, *Acta Mater.* **54**, 3637 (2006).
- ³⁶J. P. Troadec, A. Gervois, and L. Oger, *Europhys. Lett.* **42**, 167 (1998).
- ³⁷A. Vegiri and C.-P. E. Varsamis, *J. Chem. Phys.* **120**, 7689 (2004).
- ³⁸X. W. Fang, C. Z. Wang, S. G. Hao, M. J. Kramer, Y. X. Yao, M. I. Mendeleev, Z. J. Ding, R. Napolitano, and K. M. Ho (unpublished).